Mol Neurobiol
DOI 10.1007/s12035-014-8814-6

Glutamate Release Machinery Is Altered in the Frontal Cortex of Rats with Experimental Autoimmune Encephalomyelitis

Natalí L. Chanaday · A. Alejandro Vilcaes · Ana L. de Paul · Alicia I. Torres · Alicia L. Degano · German A. Roth

Received: 22 April 2014 / Accepted: 11 July 2014

Abstract Experimental autoimmune encephalomyelitis (EAE) is an animal model that mimics many of the clinical and pathological features of the human disease multiple sclerosis (MS). Both are inflammatory demyelinating and neurodegenerative pathologies of the central nervous system associated with motor, sensory, and cognitive deficits. In MS, gray matter atrophy is related to the emergence of cognitive deficits and contributes to clinical progression. In particular, prefrontal cortex injury and dysfunction have been correlated to the development of fatigue, one of the most common and disabling symptoms in MS. However, the molecular bases of these changes remain unknown. Taking advantage of EAE similitude, we herein analyze functional and morphological changes in isolated cortical presynaptic terminals (synaptosomes) from an acute rat model. We found impaired glutamate release in the frontal cortex from EAE rats. This defect appeared along with the onset of the disease, reversing when clinical signs were no more evident. Biochemical analysis of EAE synaptosomes revealed alterations in the presynaptic release machinery and in the response to depolarization, which was accompanied by abnormal synapsin I phosphorylation and dispersion. These changes were associated with reduced synaptic vesicle mobility, with no alterations in synaptosomal morphology as evidenced by electron microscopy. The present are the first pieces of evidence unraveling the molecular mechanisms of frontal cortex neuronal dysfunction in EAE and, possibly, MS.

Keywords Experimental autoimmune encephalomyelitis · Multiple sclerosis · Synapsin · Glutamate release · Synaptosomes · Release machinery

Abbreviations

4-AP	4-Aminopyridine
BSA	Bovine serum albumin
CaMKII	Ca^{2+}/calmodulin-dependent protein kinase II
CFA	Complete Freund's adjuvant
CN	Calcineurin
CNS	Central nervous system
dpi	Days postinduction
EAE	Experimental autoimmune encephalomyelitis
Erk1/2	Extracellular signal-regulated protein kinases 1 and 2
HBM	HEPES-buffered medium
mAb	Monoclonal antibody
MS	Multiple sclerosis
pAb	Polyclonal antibody
PBS	Phosphate-buffered saline
PPD	Postsynaptic density
RRP	Readily releasable pool
SM	Synaptic membrane
SVs	Synaptic vesicles
SynI	Synapsin I

Electronic supplementary material The online version of this article (doi:10.1007/s12035-014-8814-6) contains supplementary material, which is available to authorized users.

N. L. Chanaday · A. A. Vilcaes · A. L. Degano · G. A. Roth (✉)
Centro de Investigaciones en Química Biológica de Córdoba (CIQUIBIC, CONICET-UNC), Departamento de Química Biológica, Facultad de Ciencias Químicas, Universidad Nacional de Córdoba, X5000HUA Córdoba, Argentina
e-mail: garoth@fcq.unc.edu.ar

A. L. de Paul · A. I. Torres
Centro de Microscopía Electrónica-INICSA (CONICET-UNC), Facultad de Ciencias Médicas, Universidad Nacional de Córdoba, X5000HUA Córdoba, Argentina

Published online: 19 July 2014

Introduction

Multiple sclerosis (MS) is an autoimmune disease of unknown etiology that affects the central nervous system (CNS) and leads to motor, sensory, and cognitive deficits. It is characterized by inflammation, blood-brain barrier disruption, reactive gliosis, and neurodegeneration [1], features reproduced by its animal model, experimental autoimmune encephalomyelitis (EAE). EAE can be actively induced in susceptible animals by immunization with whole myelin or specific myelin proteins in an appropriate adjuvant. This model has been widely used to study the molecular and cellular basis of MS as well as to design or validate new strategies for treatment [2, 3]. Nevertheless, MS and classic EAE differ in the pattern of lesion distribution within the CNS. While most MS patients exhibit lesions primarily in the brain, animals with classic EAE present the majority of inflammatory plaques in the spinal cord and optic nerve [4]. Therefore, most of EAE research has historically focused on spinal cord neuroinflammation. In the last years, the relevance of cortical damage and neurodegeneration in MS has grown, since it may be the major contributor to irreversible disease progression and emergence of cognitive deficits [5, 6]. Although the whole brain is affected, more pronounced changes have been found in specific cortical and subcortical regions, each associated with different clinical manifestations [5]. One of the first regions showing changes at the beginning of the disease is the frontal cortex, where focal lesions, demyelination, and functional alterations were associated to cognitive decline and fatigue [7–9]. In classic EAE models, inflammation and neurodegeneration have been described in the cerebellum and deep brain structures like the striatum and the hippocampus [10–12], but the participation of the cortex has been poorly explored.

L-Glutamate is the major excitatory neurotransmitter within the CNS. Glutamatergic nerve terminals compose around 80 % of synapses in murine frontal cortex [13] and represent intracortical connections as well as projections from basal ganglia and thalamus [14]. Previous work from our group showed impaired Ca^{2+}-dependent glutamate release from cortical synaptosomes in rats with EAE, which was associated with a failure in synapsin I phosphorylation and a loss of GABAergic regulation [15, 16]. Since functional changes and atrophy in the frontal cortex may play a crucial role in MS progression, in the present work, we took advantage of EAE similitude in order to explore the molecular mechanisms underlying synaptic alterations in this pathology. These results may have broad implications for understanding the mechanism of cortical neuronal dysfunction in EAE and MS.

Materials and Methods

Chemicals

Whole myelin was purified from bovine spinal cords as previously described [17]. Complete Freund's adjuvant (CFA), bovine serum albumin (BSA), glutamate dehydrogenase (EC 1.4.1.3), $NADP^+$, and 4-aminopyridine (4-AP) were from Sigma-Aldrich Co. (St. Louis, MO, USA). Percoll was purchased from GE Healthcare Bio-Sciences (Pittsburgh, PA, USA). Neuronal class III β-tubulin (TUJ1) mouse monoclonal antibody (mAb) (MMS-435P) was from Covance, Inc. (Princeton, NJ, USA). Synapsin I (SynI)-specific mouse mAb (SM3651) was from ECM Biosciences LLC (Versailles, KY, USA). SynI phospho-sites 4/5 (Ser62/67) rabbit polyclonal antibody (pAb) (p1560-6267) was from PhosphoSolutions (Aurora, CO, USA). SynI phospho-site 3 (Ser 603) rabbit pAb (RU19) was gently provided by Dr. Paul Greengard (Laboratory of Molecular and Cellular Neuroscience, The Rockefeller University, NY, USA; see Menegon et al. [18]). p44/42 MAP kinase (extracellular signal-regulated protein kinases 1 and 2 (Erk 1/2)) rabbit pAb (9102), phospho-p44/42 MAP kinase (Thr202/Tyr204) rabbit pAb (9101), Ca^{2+}/calmodulin-dependent protein kinase II (CaMKII) (pan) (D11A10) rabbit mAb (4436), and phospho-CaMKII (Thr286) rabbit pAb (3361) were from Cell Signaling Technology, Inc. (Danvers, MA, USA). Calcineurin pan A rabbit pAb (AB1695) and GAD 65/67 rabbit pAb (AB1511) were from Chemicon International, Inc. (Temecula, CA, USA). VGluT1 rabbit pAb (135302) was from Synaptic Systems (Göttingen, Germany). All other chemicals were analytical-grade reagents of the highest purity available.

Experimental Design

Albino rats, 40 day old from a Wistar strain inbred in our laboratory for 40 years were used. All experiments were performed in accordance with the international and institutional guidelines for animal care, and the protocol was approved by the local institutional review committee for animal studies (Exp. No. 15-99-40426). Active disease was induced by intradermal injection in both hind feet of 0.5 ml of an emulsion of 0.25 ml phosphate-buffered saline (PBS) and 0.25 ml CFA containing 8 mg bovine myelin (EAE group). Control animals received 0.5 ml of the same emulsion without any antigenic preparation (CFA group). Animals were weighed and examined daily for clinical signs of neurological impairment. The animals developed only a monophasic course (acute stage, 11–13 days postinduction, dpi) and showed spontaneous neurological improvement 2–4 days after the onset of the disease, regaining the total ability to walk by 17–18 dpi [19]. Clinical severity was scored as follows: 0, no clinical expression of the disease; 0.5, loss of tip tail tonus;

1, flaccid tail; 2, hind limb weakness; 3, complete hind leg paralysis accompanied by urinary incontinence; 4, quadriparesis; and 5, moribund state or death. Animals were sacrificed at different times after onset (11–14 dpi) and during the recovering period (20–30 dpi).

Preparation of Synaptosomes and Posterior Subfractioning

Animals were sacrificed by rapid decapitation, brains were removed, and the frontal cortex and the rest of the cortex were dissected. Synaptosomes were purified on discontinuous Percoll gradients as described previously [20]. The interface between 10 and 23 % Percoll layers, corresponding to the synaptosomal fraction, was collected and diluted in a final volume of 20 ml of 4-(2-hydroxyethyl)-1-piperazineethanesulfonic acid (HEPES) buffer medium (HBM; 140 mM NaCl, 5 mM KCl, 5 mM $NaHCO_3$, 1 mM $MgCl_2$, 1.2 mM Na_2HPO_4, 10 mM glucose, and 10 mM HEPES, pH=7.4) before centrifugation at 27,000×*g* for 10 min at 4 °C. The pellets thus formed were resuspended in 2–3 ml of HBM, and protein content was determined by Bradford assay (Bio-Rad, Hercules, CA, USA). Synaptosomal pellets were stored on ice and used within 3–4 h.

A synaptosomal subfractioning method was design based on that described by Huttner et al. [21]. To obtain synaptic vesicles (SVs) and the synaptic membrane (SM), 1 ml of the synaptosomal pellet was subjected to osmotic shock by adding 9 ml of MilliQ water and homogenized for 2 min using a glass-Teflon homogenizer. HEPES/NaOH 10 mM (pH=7.4) was then added, and samples were incubated at 4 °C for 30 min. After centrifugation at 25,000×*g* for 20 min at 4 °C, the pellet (corresponding to SMs) was resuspended in sample buffer, and the supernatant was centrifuged again at 200,000×*g* for 1.5 h at 4 °C, to pellet SVs. Samples were stored in sample buffer at 4 °C until Western blotting was performed.

Glutamate Release Assay

Glutamate release was monitored by on-line fluorimetry of NADPH generated by exogenous glutamate dehydrogenase. Synaptosomal pellets were resuspended in HBM and incubated in a stirred and thermostated cuvette maintained at 37 °C in a FluoroMax-P Horiba Jobin Yvon spectrofluorometer. $NADP^+$ (1 mM), 50 units/ml glutamate dehydrogenase, and 1.2 mM $CaCl_2$ were added after 3 min. After 5 min of incubation, 3 mM 4-AP was added to stimulate glutamate release as previously described [16, 22]. Traces were calibrated by the addition of 4 nmol of glutamate at the end of each assay. Data points were obtained at 1-s intervals. Ca^{2+}-free medium with 10 μM $CdCl_2$ was used to measure Ca^{2+}-independent release. The initial rate of release was calculated as the slope of the linear approximation of the first 2 min of release.

Immunofluorescence of Synaptosomes

The protocol was based on the method described by Millán et al. [13]. Eighty microliters of synaptosomal suspension was allowed to attach to polylysinated coverslips for 45 min at room temperature. Five hundred microliters of 4 % *p*-formaldehyde in PBS (pH=7.4) was used for fixation, and after three 10-min washes with PBS, samples were pretreated for 15 min with 0.1 % Triton X-100 and 1 M glycine in PBS (for permeabilization and diminishing background fluorescence, respectively). Coverslips were washed again; then primary antibodies were added (anti-SynI 1:500; anti-GAD65/67 1:1,000; anti-VGluT1 1:1,000) in 0.1 % Triton X-100 and 1 % BSA in PBS and incubated over night at 4 °C in a humidified chamber. After three 10-min washes with PBS, secondary antibodies (anti-mouse-FITC 1:100; anti-rabbit-Cy3 1:500) were incubated for 1 h at room temperature in a humidified chamber. Coverslips were washed several times and mounted in a slide using FluorSave Reagent (Calbiochem, Merck Millipore, Darmstadt, Germany). Synaptosomes were viewed in an FV300 (Olympus) microscope with×60 objective. For colocalization analysis, ImageJ software (NIH) was employed. Briefly, images were binarized, and red and green channels were multiplied. The resulting image was subjected to particle counting restricted only to rounded particles with a diameter between 0.5 and 1.5 μm.

Western Blotting

Synaptosomal samples were resuspended in HBM with 1.2 mM $CaCl_2$ and incubated at 37 °C. After 5 min, 3 mM 4-AP was added to stimulate Ca^{2+}-dependent phosphorylation pathways concomitant to glutamate release. At different times, aliquots were rapidly solubilized in sample buffer, and equal amounts of protein were subjected to SDS-PAGE and then electrotransferred onto nitrocellulose membranes [16]. Immunoblotting was performed with phospho-specific primary antibodies. First, antibodies against phospho-CaMKII and phospho-Erk1/2 (p44/42) were used at 1:1,000 dilutions, while antibodies against SynI phospho-sites 3 and 4/5 were used at 1:2,000. After stripping the membranes with NaOH 1 M for 10 min at room temperature, immunoblotting was repeated to label total proteins; an antibody against Erk1/2 was used at 1:500, while antibodies against SynI, synaptophysin, and CaMKII pan were used at 1:1,000. Immunoreactive bands were detected by infrared probe-labeled secondary antibodies followed by scanning in an Odyssey imager (LI-COR Inc., Lincoln, NE, USA). Fluorescence intensity was quantified using GelAnalyzer 2010a software. Phosphorylated protein signals were normalized to the corresponding total protein, and total protein content was normalized to βIII-tubulin (TUJ1 antibody, used at 1:2,500). All results are represented as percent of control (i.e., CFA in basal

conditions), which was obtained independently for each experiment by duplicate.

Electron Microscopy

Synaptosomes were resuspended in HBM and incubated with 1.2 mM $CaCl_2$ at 37 °C for 5 min (basal condition). After that, 3 mM 4-AP was added and samples were mixed for 3 s (stimulated condition); then, the reaction was stopped by the addition of 0.1 M cacodylate buffer and centrifugation at 4 °C. Synaptosomal pellets were washed twice in 0.1 M cacodylate buffer and fixed in a mixture of 4 % formaldehyde and 2 % glutaraldehyde in 0.1 M cacodylate buffer for 2 h. Then, pellets were treated with 1 % OsO_4 for 1 h and stained in block with 1 % uranyl acetate in 0.1 M acetate buffer (pH= 5.2) for 20 min. After dehydration with a series of graded cold acetones, the pellets were embedded in Araldite. Thin sections (60 nm) were cut using a JEOL JUM-7 ultramicrotome (Nikon, Tokyo, Japan) with a diamond knife. Sections were stained with uranyl acetate/lead citrate and examined using a Zeiss Leo 906 E electron microscope equipped with a digital camera (Megaview III, Oberkochen, Germany). Twenty-five to thirty-five images were analyzed per sample in a blind fashion using ImageJ software (NIH).

Data Analysis

Data analysis was performed using Prism (GraphPad Software). Results are expressed as mean±SEM. For experiments with only one variable among groups (for example, total levels of a synaptosomal protein), one-way ANOVA was applied. If it revealed significant effects ($p \leq 0.05$) a pair-wise comparison of means of all groups with respect to the control group (CFA) was carried out (Dunnett's multiple comparison test). For experiments with two variables (one of which is a time or basal/stimulated condition), two-way ANOVA was employed and Bonferroni posttest was used to compare all conditions for each variable. In all the cases, a $p \leq 0.05$ was considered to represent a significant difference between groups.

Results

Glutamate Release Is Reduced in Frontal Cortex Synaptosomes from EAE Rats

In order to assess synaptosomal functionality during the different stages of EAE, glutamate release was studied in three experimental groups: CFA (negative control), EAE (corresponding to rats within 24 h of clinical sign onset), and EAE Rec (rats fully recovered, clinically indistinguishable from the CFA group). The frontal region of the brain cortex was dissected from the rest, and synaptosomes were purified as stated in methods. Figure 1a shows the time course of glutamate release from frontal cortex synaptosomes after stimulation with 4-AP. Total glutamate release was decreased about 20 % in the EAE group, and the initial rate of release was also impaired (inset in Fig. 1a). This defects in glutamate release appeared along with the first signs of disease, and it reached control values when animals fully recovered (see Online Resource 1 for a detailed time course analysis). Conversely, total released glutamate as well as the initial rate of release was similar for all experimental groups in synaptosomes purified from the remaining portion of the cortex (Fig. 1b). These results suggest that the release machinery is defective in synaptosomes from EAE rats at the onset of clinical signs, and these alterations appear to be restricted to the frontal portion of the rat cortex.

Ca^{2+}-Independent Release and Total Glutamate Content Remained Unaltered in EAE Synaptosomes

To further characterize glutamate release in synaptosomes from rats with EAE, we evaluated whether the defect was related to Ca^{2+}-dependent or independent components of release. For this, we preincubated the synaptosomal samples with the broad calcium channel blocker $CdCl_2$ and then performed the glutamate release assay with 4-AP in the absence of external Ca^{2+}. As shown in Fig. 1c, Ca^{2+}-independent release was comparable for all groups, pointing out that only the Ca^{2+}-dependent component of release was affected. In addition, the total glutamate content of synaptosomes was similar among all the experimental groups (Fig. 1d).

We also analyzed the composition of the synaptosomal preparations used for glutamate release experiments. For this, the content of GABAergic (GAD65/67-positive) and glutamatergic (VGluT1-positive) synaptosomes was quantified by immunofluorescence (Fig. 2). The composition was similar among all the groups (~80 % glutamatergic and ~10 % GABAergic synaptosomes), and it was uniform between the frontal portion and the rest of the cortex (see Online Resource 2). These results are consistent with previous reports from Wistar rat cortical synaptosomes [13]. Altogether, our data suggest that Ca^{2+}-triggered exocytic pathways are dysfunctional at the frontal cortex of EAE rats, and it could contribute to the observed reduction in glutamate release. Hence, the next experiments were addressed to test this hypothesis.

Synapsin I Phosphorylation and Redistribution Is Altered in EAE

Syns are a family of neuron-specific phosphoproteins and the most abundant of presynaptic proteins. They regulate the number of SVs and their retention at presynaptic terminals,

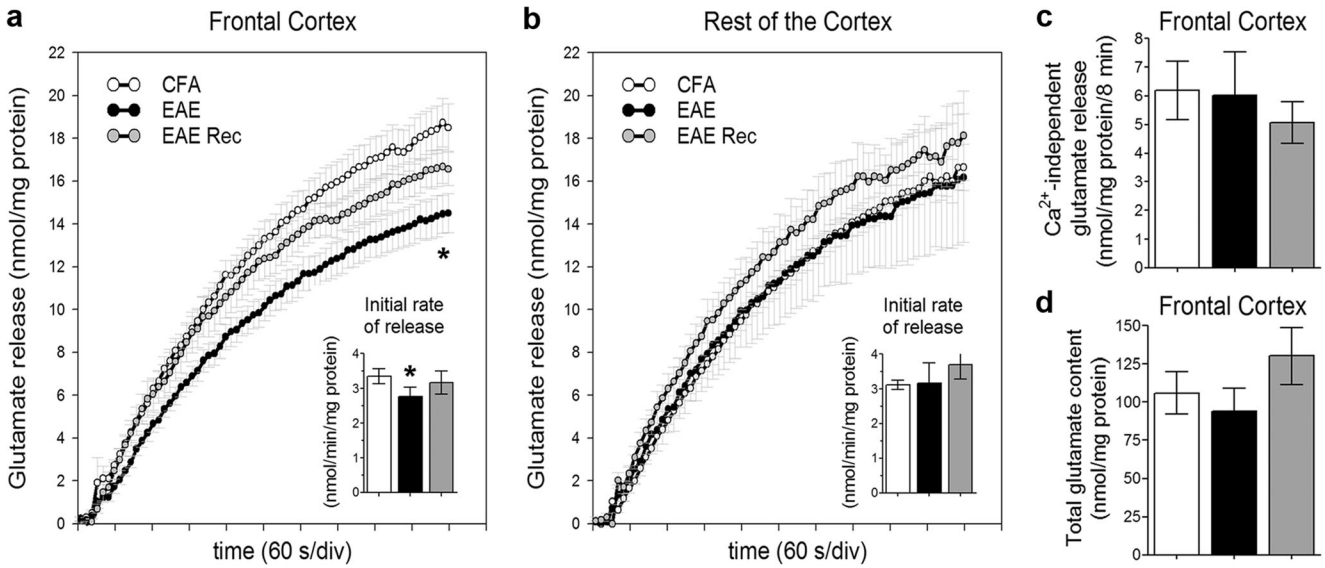

Fig. 1 4-AP-induced glutamate release from synaptosomes of the frontal region and the rest of the cortex: characteristics and components. **a** Time course of glutamate release from frontal cortex synaptosomes. Total released glutamate results from the sum of Ca^{2+}-dependent and Ca^{2+}-independent releasing mechanisms. EAE (*black circle*) curve is clearly shifted with respect to control (CFA; *white circle*) and recovered EAE (EAE Rec; *gray circle*) curves. Total glutamate release values: CFA=17.9±0.9 nmol/mg protein, EAE=14.3±0.8 nmol/mg protein, and EAE Rec=16.8±0.6 nmol/mg protein. *Inset*: initial rate of glutamate release (first 2 min), CFA=3.3±0.2 nmol/mg protein * min, EAE=2.7±0.2 nmol/mg protein * min, and EAE Rec=3.2±0.4 nmol/mg protein * min. **b** Time course and initial rate of glutamate release from synaptosomes of the rest of the cortex. **c** 4-AP-induced glutamate release from frontal cortex synaptosomes in the absence of external Ca^{2+} and presence of $CdCl_2$. The similitude among the groups in this type of release indicates that only Ca^{2+}-dependent release is affected in EAE. **d** The glutamate content of frontal cortex synaptosomes is similar among the groups. *Frontal cortex*: Data from five independent experiments (N=ten rats per group) are expressed as mean±SEM (*$p \leq 0.05$). *Rest of the cortex*: Data from three independent experiments (N=six rats per group) are expressed as mean±SEM (one-way ANOVA and Dunnett's multiple comparison test)

controlling SV availability for exocytosis [23]. SynI was the first member of this family being discovered, and it has been the most extensively studied. We evaluated SynI protein amount by Western blot in frontal cortex synaptosomes from control and EAE rats (Fig. 3b). SynI levels were similar for all experimental groups, indicating that the expression/degradation ratio for this protein is not altered during EAE.

SynI phosphorylation at different sites regulates SV availability and actin dynamics [24, 25]. Phosphorylation at sites 2 and 3 by CaMKII has a strong conformational effect that negatively regulates vesicle affinity as well as actin interaction, allowing vesicle mobilization and fusion at the active zone (AZ; Chi et al. [26]). We tested the phosphorylation levels of SynI at site 3 in frontal cortex synaptosomes by Western blot. While basal phosphorylation levels of SynI at site 3 were similar among the experimental groups, the phosphorylation at this site induced by 4-AP depolarization was significantly diminished in frontal cortex synaptosomes from rats with EAE (Fig. 3c). Phosphorylation at site 3 peaked at 1 min after 4-AP addition; at that time point, the EAE group reached only half the levels observed for the CFA group.

The ability of SynI to modulate actin dynamics (but not its affinity for SVs) is also regulated by phosphorylation at sites 4, 5, and 6 by Erk1/2 (Chi et al. [26]). In contrast to the phosphorylation pattern observed for site 3, basal phosphorylation of SynI at sites 4/5 as well as the phosphorylation induced by 4-AP after 1 min (peak) were increased in synaptosomes from the EAE group (Fig. 3d). Importantly, the level of SynI phosphorylation at the mentioned sites was similar in fully recovered animals (EAE Rec) and in the CFA group.

To further understand the implications of these findings, we performed a synaptosomal subfractioning to separate the SVs from SM (which includes synaptosomal plasma membrane as well as docked vesicles and other associated proteins and structures). The reliability of the technique was confirmed by characterization of the different fractions using specific protein markers (see Online Resource 3). When synaptosomes from the control group (CFA) were stimulated for 1 min with 4-AP, SynI levels decreased about 40 % in SVs and 30 % in SM fractions (white bars in Fig. 3g, h). These findings are in agreement with previous reports indicating that first, SynI is released from SVs upon stimulation; second, SynI is also present in membrane-associated vesicles; third, a proportion of SynI remains attached to SVs [27]. SynI detachment from vesicles was impaired in the EAE group after stimulation, since no significant decrease was observed in SVs and SM (black bars in Fig. 3g, h). These alterations in SynI redistribution were reverted in recovered animals (gray bars in Fig. 3g, h; note that basal levels of SynI bound to SVs are

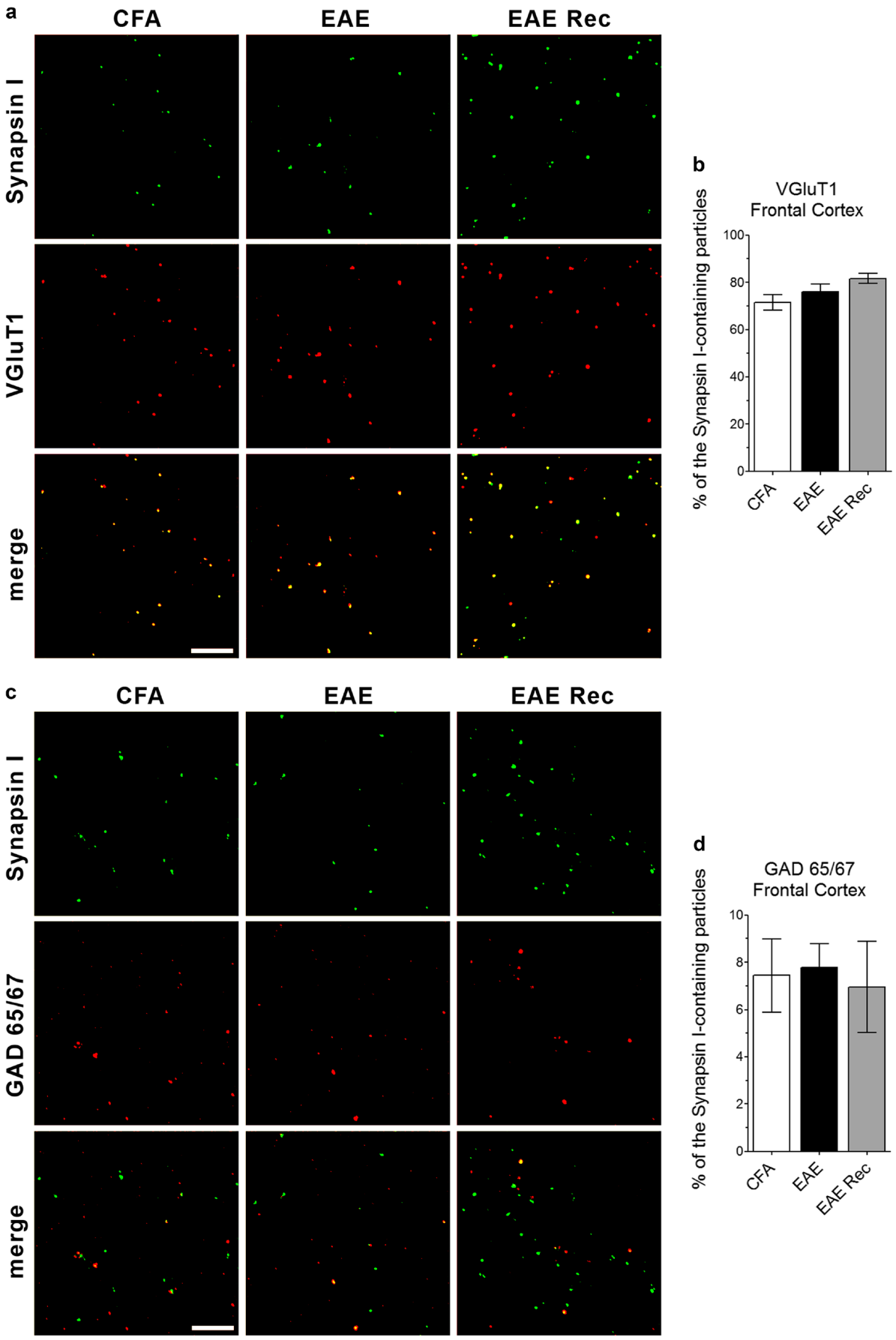
a
CFA
EAE
EAE Rec
Synapsin I
VGluT1
merge
b
VGluT1
Frontal Cortex
% of the Synapsin I-containing particles
100
80
60
40
20
0
CFA
EAE
EAE Rec
c
CFA
EAE
EAE Rec
Synapsin I
GAD 65/67
merge
d
GAD 65/67
Frontal Cortex
% of the Synapsin I-containing particles
10
8
6
4
2
0
CFA
EAE
EAE Rec

◀ **Fig. 2** Characterization of synaptosomal preparation by immunofluorescence. SynI antibody was used to identify the total number of synaptosomes. Particles showing colocalization of VGluT1 or GAD65/67 with SynI were defined as glutamatergic or GABAergic synaptosomes, respectively. Values are shown as percentage of VGluT1+ or GAD65/67+ synaptosomes relative to total synaptosomes and expressed as mean±SEM. **a**, **b** Percent of GABAergic synaptosomes: CFA=7.4±1.5 %, EAE=7.7±1.0 %, and EAE Rec=7.0±1.9 %. **c**, **d** Percent of glutamatergic synaptosomes: CFA=71.5±3.3 %, EAE=76.0±3.2 %, and EAE Rec=81.6±2.1 % (due to ~10 % variability among independent experiments, there are no significant differences). The composition of all samples was similar. Data from five independent experiments (*N*=five rats per group; ten images per sample were analyzed; one-way ANOVA and Dunnett's multiple comparison test)

increased in the EAE Rec group, possibly indicating an adaptive response).

In summary, the pattern of SynI phosphorylation is altered in nerve terminals from the frontal cortex of EAE rats. This defect leads to failure in SynI detachment from SVs and might be altering the cycling of SVs in the presynaptic terminal.

Synapsin I Partners: Release Machinery Is Modified During EAE

As mentioned before, SynI dynamics is regulated by a number of protein kinases and phosphatases that participate in the transduction of signals (such as action potentials or chemical mediators) to trigger neurotransmitter release. In order to elucidate the mechanism behind the alterations observed in SynI and glutamate release in EAE, we next studied CaMKII and Erk1/2 function under resting and stimulated conditions in frontal cortex synaptosomes.

The kinase that phosphorylates sites 2 and 3 of SynI, CaMKIIα, had similar protein levels in whole synaptosomes from all the groups (Fig. 4b). After stimulation with 4-AP for 8 min, these levels remained constant, indicating that there is no significant CaMKIIα synthesis or degradation in our experimental conditions (data not shown). In resting presynapsis, CaMKIIα has a peripheral localization, whereas it is redistributed to SV clusters and AZ after depolarization, through a process dependent on Ca^{2+}/calmodulin binding and autophosphorylation at Thr286 [28, 29]. In control synaptosomes (CFA) under basal conditions, we found CaMKIIα associated to SVs and to SM. After depolarization for 1 min with 4-AP, these kinase levels showed a 50 % decrease in SVs and about a 50 % increase in SM (white bars in Fig. 4e, f). These data could indicate either a redistribution of the CaMKIIα, the mobilization of this kinase along with SVs, or a combination of both processes. Although the percentage of CaMKIIα attached to SVs was similar in EAE and CFA synaptosomes after stimulation, the basal levels of this protein associated to SVs in EAE synaptosomes were about 30 % lower with respect to CFA synaptosomes (black bars in Fig. 4e). SM-bound CaMKIIα levels were similar in EAE and CFA (Fig. 4f), indicating that only the recruitment to SVs would be altered. CaMKIIα autophosphorylation levels after 4-AP stimulation were similar in CFA and EAE groups (data not shown), indicating that the protein is functional in EAE synaptosomes, and the failure in SynI site 3 phosphorylation is due to the reduced CaMKIIα associated to SV clusters. In recovered animals, basal presynaptic localization of CaMKIIα was restored, but it failed to be redistributed after depolarization (gray bars in Fig. 4e, f). This could imply that the recovery of glutamate release in EAE Rec synaptosomes might be accomplished through a different mechanism.

On the other hand, SynI phosphorylation sites 4 to 6 are substrates of Erk1/2. In agreement with the observed increase in SynI site 4/5 phosphorylations (Fig. 3d), total protein levels as well as 4-AP-induced phosphorylation of Erk1/2 were significantly augmented in frontal cortex synaptosomes from rats with EAE (Fig. 5b, c). Interestingly, calcineurin (CN) levels were also increased in the EAE group (Fig. 5f). CN is activated by rises in intracellular Ca^{2+} and dephosphorylates sites 4 to 6 of SynI. Synaptosomes from CFA frontal cortex had CN associated to SMs in resting conditions, and this amount increases after depolarization, probably due to the interaction of CN with its targets (Fig. 5g). Higher levels of CN protein were also observed in SM fractions from EAE synaptosomes (about 40 % more), but it did not increase further after 4-AP stimulation (black bars in Fig. 5g). Based on these data, although Erk1/2 and CN are both augmented, Erk1/2 activity seems to overcome CN activity resulting in SynI being more phosphorylated at sites 4/5 in EAE synaptosomes. Synaptosomes from fully recovered animals showed similar levels of Erk1/2 and CN as the control group (gray bars in Fig. 5). Altogether, our data signaling pathways that regulate SynI phosphorylation status are dysfunctional in frontal cortex synaptosomes from rats with EAE.

Morphological Analysis Confirms Reduced SV Mobility

The biochemical results support the hypothesis that SV cycling is altered in the frontal cortex during EAE onset. To further test this hypothesis, synaptosomes in resting and depolarized conditions were analyzed by electron microscopy (Fig. 6a). Synaptosomal and mitochondrial morphology was similar and well preserved in CFA and EAE samples. Particularly, the size of synaptosomes and SVs as well as the length of the postsynaptic density (PSD) were similar in both experimental groups (Fig. 6c) and comparable to previous reports [20, 30]. To assess the redistribution of SVs after 4-AP-induction, the readily releasable pool (RRP) of SVs was quantified. RRP was defined as the sum of docked SVs (i.e., vesicles whose membrane contact the AZ) and of vesicles within a 20-nm distance of the AZ. The AZ is believed to be a dense matrix of proteins and SVs, so the number of attached SVs and release sites scales with AZ size (modular model of

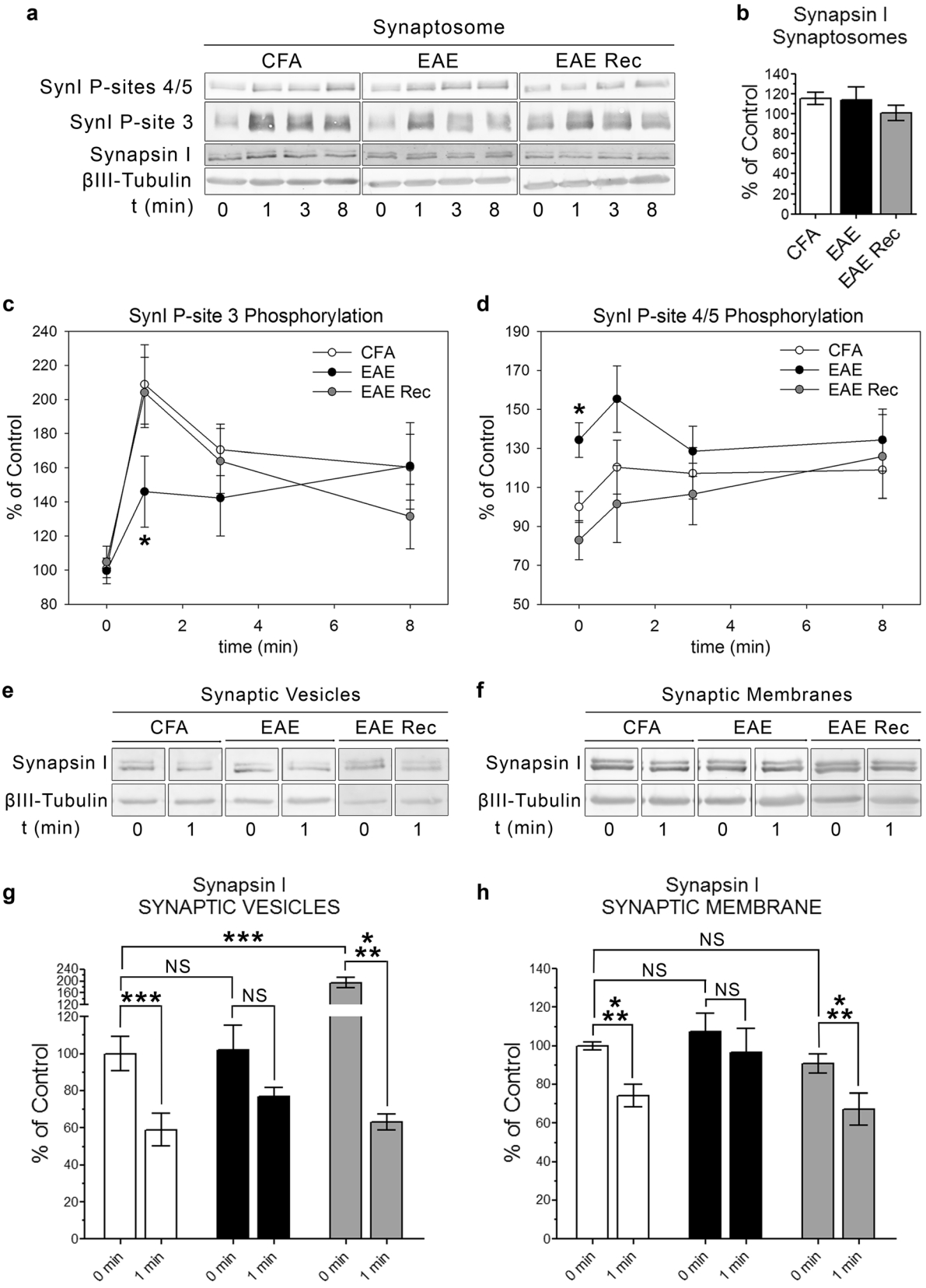
a
Synaptosome
CFA
EAE
EAE Rec
SynI P-sites 4/5
SynI P-site 3
Synapsin I
βIII-Tubulin
t (min)
0 1 3 8 0 1 3 8 0 1 3 8
b
Synapsin I
Synaptosomes
% of Control
CFA
EAE
EAE Rec
c
SynI P-site 3 Phosphorylation
% of Control
time (min)
CFA
EAE
EAE Rec
d
SynI P-site 4/5 Phosphorylation
% of Control
time (min)
CFA
EAE
EAE Rec
e
Synaptic Vesicles
CFA
EAE
EAE Rec
Synapsin I
βIII-Tubulin
t (min)
0 1 0 1 0 1
f
Synaptic Membranes
CFA
EAE
EAE Rec
Synapsin I
βIII-Tubulin
t (min)
0 1 0 1 0 1
g
Synapsin I
SYNAPTIC VESICLES
% of Control
NS
0 min
1 min
h
Synapsin I
SYNAPTIC MEMBRANE
% of Control
NS
0 min
1 min

◀ **Fig. 3** Synapsin I phosphorylation and redistribution after depolarization. **a** Representative Western blot images of synaptosomal SynI. **b** The total synaptosomal content of SynI was similar for all groups: CFA=116±6 %, EAE=114±13 %, EAE Rec=101±8 %. Per sample, SynI levels were normalized to βIII-tubulin and relativized to the CFA group. For **c** and **d**, SynI phosphorylation levels were normalized to total SynI and then relativized to the CFA group. **c** Time course of SynI phosphorylation at site 3 (*P-site 3*) in whole synaptosomes after 4-AP depolarization. At the peak (1 min) SynI P-site 3 had a value of 209± 25 % for the CFA group and 146±20 % for the EAE group, showing a failure in the phosphorylation of this site. **d** Time course of SynI phosphorylation at sites 4/5 (*P-site 4/5*) in whole synaptosomes after 4-AP depolarization. At basal condition SynI P-site 4/5 3 had a value of 100 ±8 % for the CFA group and 134±8 % for the EAE group, showing increased phosphorylation. **e**, **f** Representative Western blot images of SynI in SVs and SM. **g**, **h** Levels of SynI bound to SVs or SM before (0 min) and after (1 min) depolarization, revealing differential redistribution in the EAE group. **b**–**d** Data from three independent experiments (*N*=six rats per group). **g**, **h** Data from two independent experiments (*N*=four rats per group). Results are expressed as mean± SEM (*$p \leq 0.05$; **$p \leq 0.01$; ***$p \leq 0.001$; two-way ANOVA with Bonferroni posttest)

the AZ; Holderith et al.; Szule et al. [31, 32]). Since PSD length and therefore AZ length vary among synaptosomes in the same sample, the RRP was expressed as the number of SVs per micrometer of PSD, assuming that PSD and AZ length were equal. Following 3-s stimulation with 4-AP, the RRP increased about 25 % in the CFA group (Fig. 6b). Basal RRP size was comparable in EAE synaptosomes, but it showed a rise of only 15 % after 4-AP addition (statistically not significant from basal condition). This difference was not due to a reduction in the total pool since synaptosomal sections from CFA and EAE had similar numbers of SVs (Fig. 6c). This result points to a failure in SV cycling in EAE synaptosomes. Taken together with the biochemical experiments, these data indicate that alterations in signaling pathways controlling SV mobility may be responsible for the deficit in glutamate release from frontal cortex synaptosomes of EAE rats at the onset of clinical signs.

Discussion

In the present work, we demonstrate a dysfunction in the presynaptic glutamate release machinery coincident with the beginning of EAE clinical manifestations. This defect led to reduced SV mobility and a reduction of glutamate release upon depolarization. Furthermore, these alterations were restricted to the frontal region of the rat brain cortex and disappeared rapidly when animals recovered.

Our group has previously described a decrease in Ca^{2+}-dependent glutamate release in the cortex of symptomatic rats with acute EAE [16]. Similar results were reported by Di Prisco et al. [33] using a chronic mouse model of EAE where the reduction in cortical glutamate exocytosis persisted along with the clinical signs and was accompanied by mild inflammation and demyelination. Here, using an acute rat model of EAE, we demonstrate that changes in glutamate release were confined to the frontal region of the cortex and occur in a narrow time window, between the appearance of clinical signs and the disease recovery (resembling the acute course of the pathology; Online Resource 1). Not only total released glutamate was reduced but also the initial rate of release (Fig. 1). Glutamate content was similar in synaptosomes from CFA and EAE groups, and more interestingly, Ca^{2+}-independent glutamate release was unaffected. In addition, our previous study [16] showed similar differences in glutamate release between CFA and EAE after induction with the Ca^{2+} ionophore ionomycin, as well as comparable 4-AP-induced Ca^{2+} influx measured with Fura-2-AM in CFA and EAE groups. Taken together, our data strongly point to a dysfunction in the presynaptic release machinery rather than ion channel deregulation.

To test this hypothesis, we started by analyzing SynI, the most abundant of synaptic proteins. SynI interacts with other synapsins as well as with SVs and actin, leading to the formation of clusters and therefore controlling SV availability for exocytosis. These associations are regulated by the phosphorylation state of SynI at different sites (for review see Cesca et al. [27]). SynI phosphorylation at sites 4/5 by Erk1/2 has a dual role on neurotransmitter release. Both constitutively phosphorylated and non-phosphorylatable forms of SynI at sites 4 to 6 had detrimental effects on SV turnover [26]. Moreover, Erk1/2 negatively regulates L-type calcium channel surface expression in neurons limiting exocytosis and inhibits posttetanic potentiation in a SynI site 4/5 phosphorylation-dependent way [34, 35]. Our study shows an increase in Erk1/2 protein level as well as a more pronounced Erk1/2 phosphorylation after 4-AP addition in EAE synaptosomes (Fig. 5), concomitantly with a higher basal and stimulated level of SynI phosphorylated at sites 4/5 (Fig. 3). In cultured neurons, Giachello et al. [36] found that overexpressed SynI displays a diffuse and uniform pattern, instead of the classic punctate distribution, when it is pseudo-phosphorylated at Erk1/2 sites. Considering that phosphorylation at sites 4 to 6 only affects SynI binding to actin, but not to SVs, our results suggest that SV clusters are more disperse in resting nerve terminals during EAE, and SVs are not correctly positioned to respond to the depolarizing stimulus.

On the other hand, SynI phosphorylation at sites 1 to 3 has a negative effect on SynI association to SVs and on the kinetics of SV turnover [37]. In agreement with that, EAE synaptosomes with reduced glutamate release had less SynI phosphorylated at site 3 after depolarization (CaMKII substrate; Fig. 3) and reduced basal levels of CaMKIIα associated to SVs (Fig. 4). Accordingly, SynI site 1 (substrate for PKA and CaMKI) is also less phosphorylated during EAE [16]. These changes in the phosphorylation status occurred concomitantly with failure in SynI dispersion, which remained

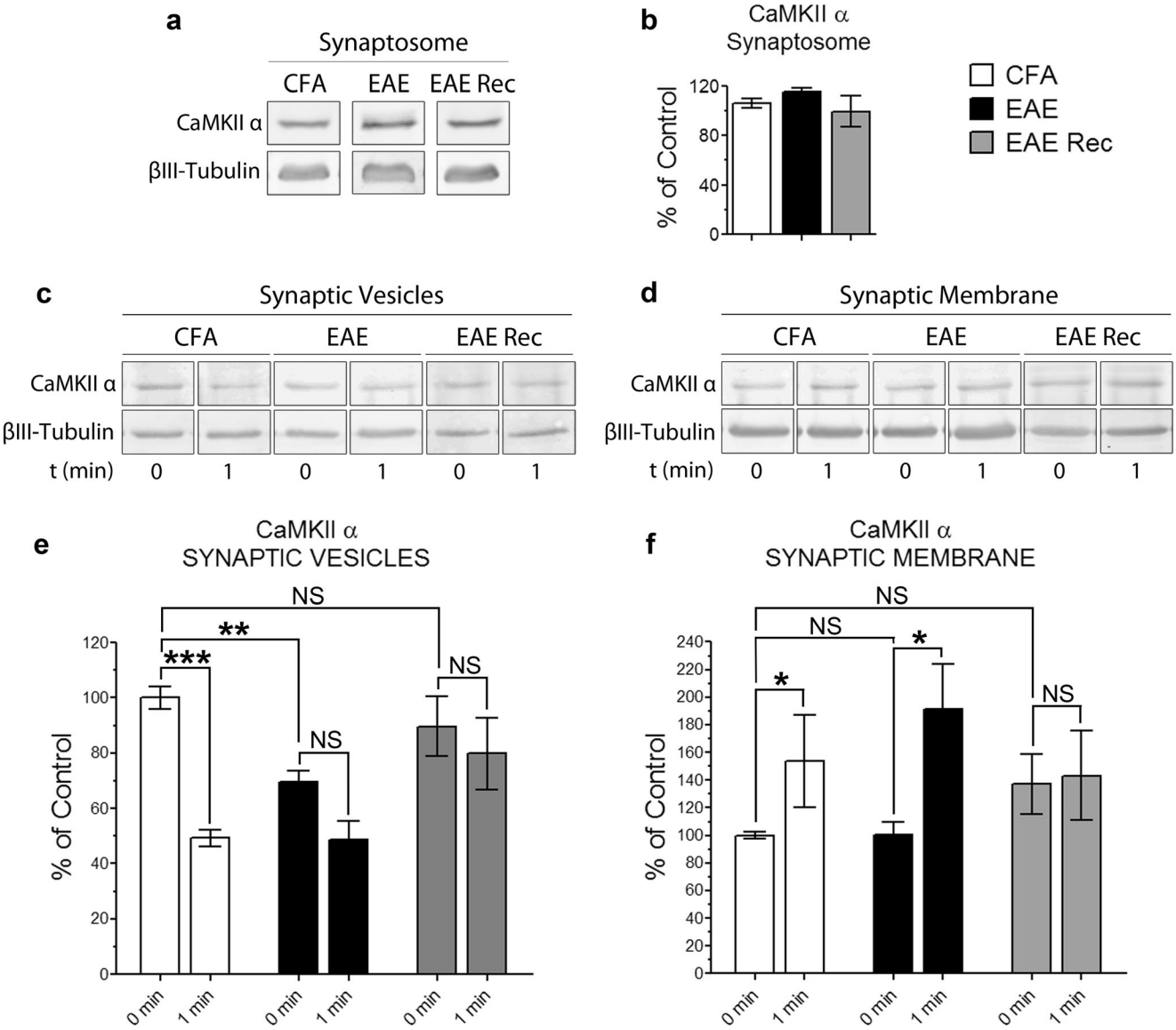

Fig. 4 CaMKIIα phosphorylation and redistribution after depolarization. **a** Representative Western blot images of synaptosomal CaMKIIα. **b** The total synaptosomal content of CaMKIIα was similar for all the experimental groups. **c**, **d** Representative Western blot images of CaMKIIα in SVs and SM. **e**, **f** Levels of CaMKIIα bound to SVs or SM before (0 min) and after (1 min) depolarization. **b** Data from three independent experiments (*N*=six rats per group). **e**, **f** Data from two independent experiments (*N*=four rats per group). Results are expressed as mean±SEM (*$p \leq 0.05$; **$p \leq 0.01$; ***$p \leq 0.001$; two-way ANOVA with Bonferroni posttest)

attached to the reserve pool as well as to docked SVs (Fig. 3). Tao-Cheng et al. [29] demonstrated that CaMKII is located around SV clusters, and it gains access to inner vesicles as peripheral vesicles are dispersed. In this context, our results in EAE synaptosomes could be explained through a model in which less basal CaMKIIα bound to SVs (Fig. 3g, black bars) leads to lower SynI site 3 phosphorylation at peripheral SVs, less dispersion of SynI and SVs, and lower penetration of CaMKIIα into the cluster. This model agrees with the reduction in SynI site 3 phosphorylation in EAE synaptosomes (Fig. 2c). Furthermore, redistribution of CaMKIIα from SVs to SM was similar in CFA and EAE groups, suggesting that

Fig. 5 Erk1/2 levels and phosphorylation after depolarization. **a** ▶ Representative Western blot images of synaptosomal Erk1/2. **b** Total synaptosomal content of Erk1/2 showing increased levels in the EAE group. **c** Time course analysis of Erk1/2 (p44/p42) phosphorylation in whole synaptosomes after 4-AP depolarization showed a significant increase in the EAE group compared to CFA. **d**, **e** Representative Western blot images of CN in whole synaptosomes and SM (respectively). **f** The total synaptosomal content of CN was increased in the EAE group. **g** Levels of CN bound to SM before (0 min) and after (1 min) depolarization. **b**, **c** Data from three independent experiments (*N*=six rats per group). **f** Data from four independent experiments (*N*=eight rats per group). **g** Data from two independent experiments (*N*=four rats per group). Results are expressed as mean±SEM (* $p \leq 0.05$; ** $p \leq 0.01$; *** $p \leq 0.001$; two-way ANOVA with Bonferroni posttest, except for **b**, where one-way ANOVA and Dunnett's multiple comparison test were applied)

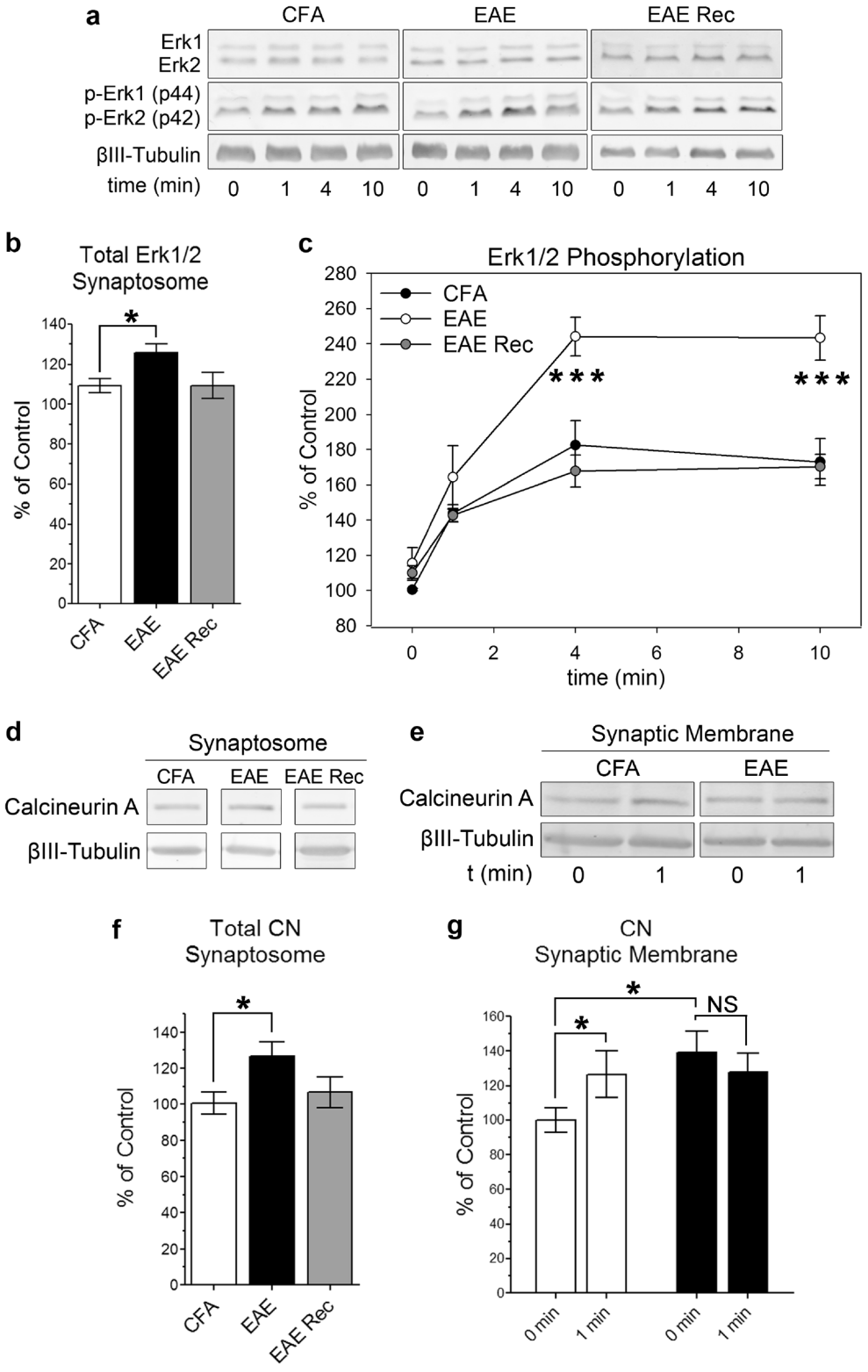

recruiting mechanisms to SV clusters, but not to the AZ, are altered during EAE (probably because of different protein composition of both structures). Also, SV recycling is dependent on actin dynamics and CN activity [38]. CN regulates the dephosphins, a group of proteins essential for the different stages of the endocytic process [39]. As discussed above, CN is increased in EAE synaptosomes, and additionally, the actin network might be unstructured as a consequence of Erk1/2

increase. Therefore, we cannot rule out the presence of alterations in endocytosis and recycling processes in EAE nerve terminals, besides the release defects described in the present work.

Electron microscopy experiments further reinforce the biochemical findings and the hypothesis of defective SV cycling. Less number of SVs reached the AZ in EAE synaptosomes after depolarization in comparison to CFA (Fig. 6), with no apparent morphological or SV content differences. Altogether, our results demonstrate that changes in the presynaptic release machinery occur in the frontal cortex during EAE. These changes involve alterations in the phosphorylation status at different sites of SynI, which converge to the same result: altered SynI-SV cluster dynamics and the consequent reduction in SV mobility and glutamate release.

Regarding the possible causes of these presynaptic molecular and functional alterations, EAE has an important inflammatory component. Immune cell infiltration and gliosis occur across the CNS accompanied with the production of inflammatory mediators, such as cytokines and glutamate, which leads to neuronal damage and excitotoxicity [1, 11]. Erk1/2 activation has been associated to the presence of infiltrates in the spinal cord of rats with acute EAE [40]. Sublethal activation of NMDA receptors in neurons generates tolerance to future excitotoxic insults through the activation of the Erk1/2 pathway [41]. Conversely, overactivation of NMDA receptors is associated to excitotoxicity and neurodegeneration in several pathology cases, including EAE and MS. In this context, anti-inflammatory cytokines like IL-6 or trophic factors like BDNF display neuroprotective effects. This is accomplished via activation of Erk1/2 and its downstream effectors [42, 43]. In this work we showed an increase in Erk1/2 levels in EAE synaptosomes (Fig. 5) which might reflect a neuroprotective neuronal response to excitotoxicity. We also found higher levels of CN, the phosphatase that acts on SynI sites that are substrates for Erk1/2. Glial CN is strongly induced by cytokines. In neurons, the pro-inflammatory cytokine TNF-α triggers Ca^{2+} release from intracellular stores and CN activation, which, in turn, promotes NFAT nuclear translocation and FasL/Fas apoptotic pathway activation [44, 45]. CN inhibitors have immunosuppressive effects and are used to diminish organ rejection after transplantation [46]. Thus, it is very likely that the observed increment in CN and Erk1/2 levels in frontal cortex synaptosomes at the beginning of EAE is a result of inflammation and/or excitotoxicity and could explain why the described changes disappear with the onset of EAE recovery. More experiments are being performed to assess this hypothesis. Unpublished data from our group indicate the presence of focal inflammation in specific CNS areas accompanied by reduction in synaptosomal glutamate release in the surroundings (besides frontal cortex, we found alterations in areas like the caudate putamen and the cerebellum).

Beyond some anatomical differences, human, macaque, and rat frontal lobes share functional properties and network connectivity [47–49]. The frontal cortex has been implicated in higher cognitive processes [50] which are achieved by the interaction of the prefrontal cortex, the basal ganglia, and the thalamus. Dysfunction of one of these regions or the connectivity between them has been associated to the development of central fatigue [51], one of the most common and disabling symptoms in MS [52]. Interestingly, although fatigue score does not correlate with disability status or disease stage in MS patients [53], several authors did find an association between fatigue score and the degree of prefrontal cortex injury in MS [9, 54]. On the other hand, cognitive decline in this pathology was related to cortical atrophy, functional changes, and connectivity loss [5, 8, 55]. Progressive synaptic and neuronal loss in the cortex of mice with chronic EAE was also found by magnetic resonance imaging [6]. Nevertheless, little is known about the mechanism behind neuronal dysfunction in these areas. Na^{+} accumulation as consequence of axonal ion exchanger malfunctioning and mitochondrial exhaustion after demyelination has been described in brains of patients with MS [56]. Roelcke et al. [57] found reduced glucose metabolism in the frontal cortex and basal ganglia associated with the presence of severe fatigue in MS. Our group reported synaptic alterations in the cortex of rats with EAE, namely a decrease in Ca^{2+}-dependent glutamate release accompanied by a failure in SynI phosphorylation and a diminution in surface $GABA_A$ receptor density [15, 16]. In the present work, we extend those findings to show that presynaptic alterations are confined to the frontal region of the cortex and consist of a dysregulation of the release molecular machinery which leads to impaired SV mobility and reduction in neurotransmitter release.

In models of classic EAE, areas like the cerebellum, the striatum, and the hippocampus have been generally studied [10, 11, 58], but the frontal cortex has been poorly explored. Although it has been widely considered that this experimental pathology affects mainly the spinal cord, previous work from our group showed that induced rats that do not develop EAE still have inflammation, demyelination, and biochemical alterations in the spinal cord (subclinical EAE; Scerbo et al. [3]), pointing us to think that unknown brain changes may contribute to the manifestation of clinical signs. The dysfunction in frontal cortex nerve terminals described here might be one of these unknown contributors to the development of EAE and also could participate in the appearance of irreversible cognitive damage. In this regard, we are currently extending these findings with the study of the relationship of frontal cortex dysfunction with the appearance and recovery of EAE symptoms, with special focus on fatigue and cognitive performance in pre- and postepisode stages.

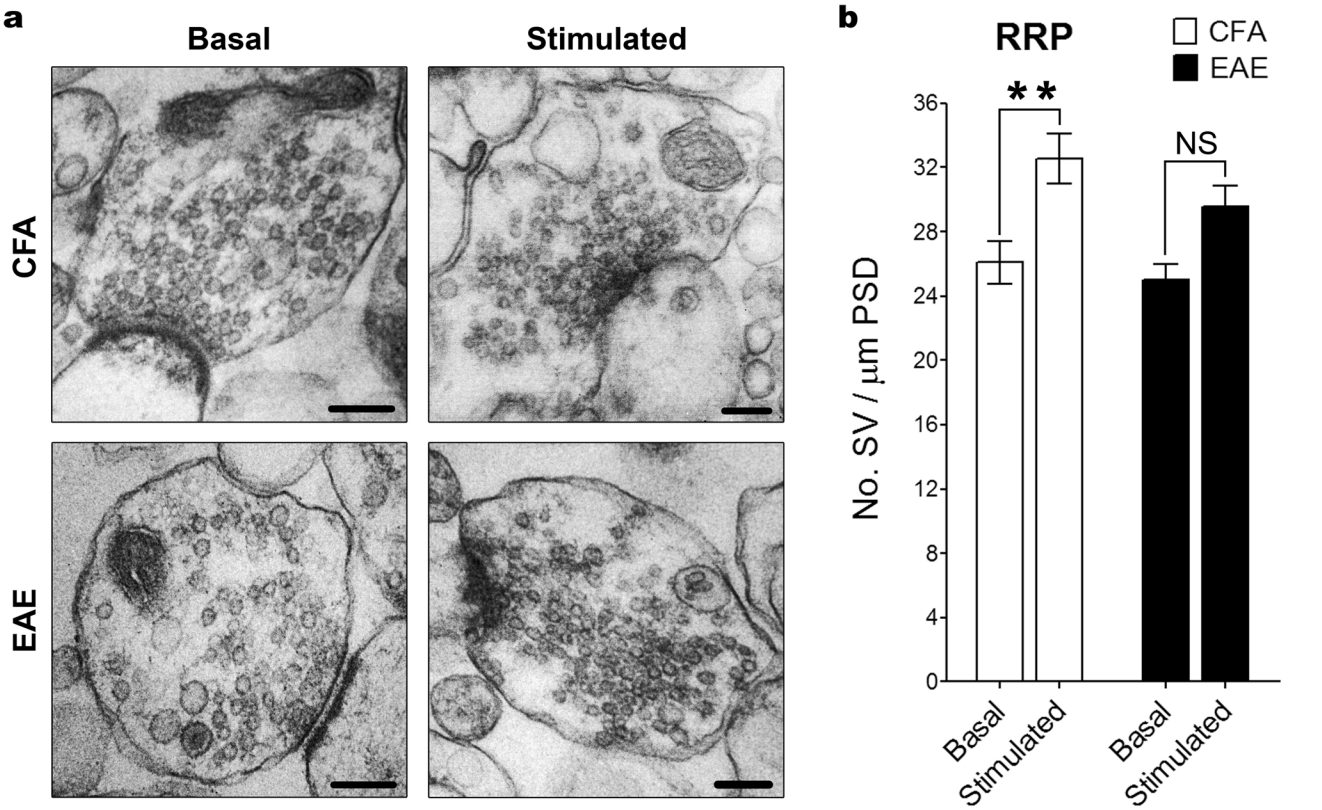

c

Group and condition	Synaptosome section diameter (µm)	SV diameter (nm)	No of SVs per synaptosomal section	PSD length (µm)
CFA - Basal	0.89 ± 0.04	42.1 ± 0.9	82 ± 6	0.28 ± 0.01
CFA - Stimulated	0.83 ± 0.03	40.1 ± 0.7	82 ± 4	0.27 ± 0.01
EAE - Basal	0.90 ± 0.03	39.8 ± 0.7	90 ± 4	0.28 ± 0.01
EAE - Stimulated	0.85 ± 0.02	40.8 ± 0.8	86 ± 4	0.28 ± 0.01

Fig. 6 Electron microscopy of synaptosomes. **a** Representative images of synaptosomes from CFA and EAE groups. *White bar*=250 nm. **b** RRP size before (*basal*) and after (*stimulated*) 4-AP-depolarization. RRP was defined as the number of SVs within 20 nm from the membrane, per micrometer of PSD. 4-AP induced an increment in RRP size in CFA synaptosomes (*white circle*): 26±1 vesicles per micrometer at resting state and 32±1 vesicles per micrometer after depolarization. This process failed in EAE synaptosomes (*black circle*): 25±1 vesicles per micrometer at resting state and 29±1 vesicles per micrometer after depolarization. **c** Morphological characteristics of synaptosomes and SVs, showing no differences between groups. Data from two independent experiments (N=two rats per group, 25–35 images were analyzed per sample) and expressed as mean±SEM (**$p \leq 0.01$; two-way ANOVA with Bonferroni posttest)

In conclusion, to our knowledge, this is the first time that presynaptic molecular pathways involved in neuronal dysfunction in the frontal cortex are explored in EAE. Further research will be needed to link accurately these alterations to the initial causes, most probably inflammatory mediators and/or demyelination, and to understand in detail their clinical and cognitive consequences. Due to the similitude between EAE and MS, the same mechanisms might be responsible for functional abnormalities in patients' frontal cortex and could contribute to the development and progression of cognitive impairment and fatigue.

Acknowledgments We wish to thank Dr. José Sánchez-Prieto (Departamento de Bioquímica, Facultad de Veterinaria, Universidad Complutense, Madrid, Spain) for his valuable advises regarding immunofluorescence of synaptosomes. We thank Dr. Paul Greengard, Dr. Angus Nairn, and Shuk Kei Cheng (Laboratory of Molecular and Cellular Neuroscience, The Rockefeller University, NY, USA) for gently providing us the SynI P-site 3 antibody (RU19). We thank Dr. Cecilia Sampedro

and Dr. Alejandra Trenchi for guiding us with microscope handling and image analysis. This work was supported by Consejo de Investigaciones Científicas y Técnicas (CONICET), Agencia Nacional de Promoción Científica y Tecnológica (Préstamo BID, PICT 2011-0799), and Secretaría de Ciencia y Tecnología de la Universidad Nacional de Córdoba (SeCyT-UNC), Argentina. NLC and AAV are fellows, ALP, AIT, and ALD are career investigators, and GAR is a senior career investigator, all from CONICET.

Conflict of Interest The authors declare that they have no conflict of interest.

References

1. Dutta R, Trapp BD (2011) Mechanisms of neuronal dysfunction and degeneration in multiple sclerosis. Prog Neurobiol 93(1):1–12. doi:10.1016/j.pneurobio.2010.09.005
2. Mix E, Meyer-Rienecker H, Zettl UK (2008) Animal models of multiple sclerosis for the development and validation of novel therapies - potential and limitations. J Neurol 255(Suppl 6):7–14. doi:10.1007/s00415-008-6003-0
3. Scerbo MJ, Rupil LL, Bibolini MJ, Roth GA, Monferran CG (2009) Protective effect of a synapsin peptide genetically fused to the B subunit of Escherichia coli heat-labile enterotoxin in rat autoimmune encephalomyelitis. J Neurosci Res 87(10):2273–2281. doi:10.1002/jnr.22048
4. Simmons SB, Pierson ER, Lee SY, Goverman JM (2013) Modeling the heterogeneity of multiple sclerosis in animals. Trends Immunol 34(8):410–422
5. Filippi M, Rocca MA, Horsfield MA, Hametner S, Geurts JJ, Comi G, Lassmann H (2013) Imaging cortical damage and dysfunction in multiple sclerosis. JAMA Neurol 70(5):556–564. doi:10.1001/jamaneurol.2013.1954
6. MacKenzie-Graham A, Rinek GA, Avedisian A, Gold SM, Frew AJ, Aguilar C, Lin DR, Umeda E, Voskuhl RR, Alger JR (2012) Cortical atrophy in experimental autoimmune encephalomyelitis: in vivo imaging. Neuroimage 60(1):95–104. doi:10.1016/j.neuroimage.2011.11.099
7. Jehna M, Langkammer C, Khalil M, Fuchs S, Reishofer G, Fazekas F, Ebner F, Enzinger C (2013) An exploratory study on the spatial relationship between regional cortical volume changes and white matter integrity in multiple sclerosis. Brain Connect 3(3):255–264. doi:10.1089/brain.2012.0108
8. Sbardella E, Petsas N, Tona F, Prosperini L, Raz E, Pace G, Pozzilli C, Pantano P (2013) Assessing the correlation between grey and white matter damage with motor and cognitive impairment in multiple sclerosis patients. PLoS One 8(5):e63250. doi:10.1371/journal.pone.0063250
9. Sepulcre J, Masdeu JC, Goñi J, Arrondo G, Vélez de Mendizábal N, Bejarano B, Villoslada P (2009) Fatigue in multiple sclerosis is associated with the disruption of frontal and parietal pathways. Mult Scler 15(3):337–344. doi:10.1177/1352458508098373
10. MacKenzie-Graham A, Tiwari-Woodruff SK, Sharma G, Aguilar C, Vo KT, Strickland LV, Morales L, Fubara B, Martin M, Jacobs RE, Johnson GA, Toga AW, Voskuhl RR (2009) Purkinje cell loss in experimental autoimmune encephalomyelitis. Neuroimage 48(4):637–651
11. Centonze D, Muzio L, Rossi S, Furlan R, Bernardi G, Martino G (2010) The link between inflammation, synaptic transmission and neurodegeneration in multiple sclerosis. Cell Death Differ 17(7):1083–1091. doi:10.1038/cdd.2009.179
12. Ziehn MO, Avedisian AA, Tiwari-Woodruff S, Voskuhl RR (2010) Hippocampal CA1 atrophy and synaptic loss during experimental autoimmune encephalomyelitis, EAE. Lab Investig 90(5):774–786
13. Millán C, Luján R, Shigemoto R, Sánchez-Prieto J (2002) Subtype-specific expression of group III metabotropic glutamate receptors and Ca2+ channels in single nerve terminals. J Biol Chem 277(49):47796–47803. doi:10.1074/jbc.M207531200
14. Somogyi P, Tamás G, Lujan R, Buhl EH (1998) Salient features of synaptic organisation in the cerebral cortex. Brain Res Brain Res Rev 26(2–3):113–135
15. Cid MP, Vilcaes AA, Rupil LL, Salvatierra NA, Roth GA (2011) Participation of the GABAergic system on the glutamate release of frontal cortex synaptosomes from Wistar rats with experimental autoimmune encephalomyelitis. Neuroscience 189:337–344. doi:10.1016/j.neuroscience.2011.05.005
16. Vilcaes AA, Furlan G, Roth GA (2009) Inhibition of Ca^{2+}-dependent glutamate release from cerebral cortex synaptosomes of rats with experimental autoimmune encephalomyelitis. J Neurochem 108(4):881–890
17. Degano AL, Roth GA (2000) Passive transfer of experimental autoimmune encephalomyelitis in Wistar rats: dissociation of clinical symptoms and biochemical alterations. J Neurosci Res 59(2):283–290. doi:10.1002/(SICI)1097-4547(20000115)59:2<283::AID-JNR15>3.0.CO;2-S
18. Menegon A, Dunlap DD, Castano F, Benfenati F, Czernik AJ, Greengard P, Valtorta F (2000) Use of phosphosynapsin I-specific antibodies for image analysis of signal transduction in single nerve terminals. J Cell Sci 113(Pt 20):3573–3582
19. Slavin DA, Bucher AE, Degano AL, Soria NW, Roth GA (1996) Time course of biochemical and immunohistological alterations during experimental allergic encephalomyelitis. Neurochem Int 29(6):597–605
20. Dunkley PR, Jarvie PE, Robinson PJ (2008) A rapid Percoll gradient procedure for preparation of synaptosomes. Nat Protoc 3(11):1718–1728. doi:10.1038/nprot.2008.171
21. Huttner WB, Schiebler W, Greengard P, De Camilli P (1983) Synapsin I (protein I), a nerve terminal-specific phosphoprotein. III. Its association with synaptic vesicles studied in a highly purified synaptic vesicle preparation. J Cell Biol 96(5):1374–1388
22. Sihra TS, Bogonez E, Nicholls DG (1992) Localized Ca^{2+} entry preferentially effects protein dephosphorylation, phosphorylation, and glutamate release. J Biol Chem 267(3):1983–1989
23. Fornasiero EF, Raimondi A, Guarnieri FC, Orlando M, Fesce R, Benfenati F, Valtorta F (2012) Synapsins contribute to the dynamic spatial organization of synaptic vesicles in an activity-dependent manner. J Neurosci 32(35):12214–12227. doi:10.1523/JNEUROSCI.1554-12.2012
24. Shupliakov O, Haucke V, Pechstein A (2011) How synapsin I may cluster synaptic vesicles. Semin Cell Dev Biol 22(4):393–399. doi:10.1016/j.semcdb.2011.07.006
25. Yamagata Y (2003) New aspects of neurotransmitter release and exocytosis: dynamic and differential regulation of synapsin I phosphorylation by acute neuronal excitation in vivo. J Pharmacol Sci 93(1):22–29
26. Chi P, Greengard P, Ryan TA (2003) Synaptic vesicle mobilization is regulated by distinct synapsin I phosphorylation pathways at different frequencies. Neuron 38(1):69–78
27. Cesca F, Baldelli P, Valtorta F, Benfenati F (2010) The synapsins: key actors of synapse function and plasticity. Prog Neurobiol 91(4):313–348
28. Griffith LC, Lu CS, Sun XX (2003) CaMKII, an enzyme on the move: regulation of temporospatial localization. Mol Interv 3(7):386–403. doi:10.1124/mi.3.7.386
29. Tao-Cheng JH, Dosemeci A, Winters CA, Reese TS (2006) Changes in the distribution of calcium calmodulin-dependent protein kinase II at the presynaptic bouton after depolarization. Brain Cell Biol 35(2–3):117–124. doi:10.1007/s11068-007-9012-5
30. Leenders AG, Scholten G, Wiegant VM, Da Silva FH, Ghijsen WE (1999) Activity-dependent neurotransmitter release kinetics:

correlation with changes in morphological distributions of small and large vesicles in central nerve terminals. Eur J Neurosci 11(12):4269–4277
31. Holderith N, Lorincz A, Katona G, Rózsa B, Kulik A, Watanabe M, Nusser Z (2012) Release probability of hippocampal glutamatergic terminals scales with the size of the active zone. Nat Neurosci 15(7): 988–997. doi:10.1038/nn.3137
32. Szule JA, Harlow ML, Jung JH, De-Miguel FF, Marshall RM, McMahan UJ (2012) Regulation of synaptic vesicle docking by different classes of macromolecules in active zone material. PLoS One 7(3):e33333. doi:10.1371/journal.pone.0033333
33. Di Prisco S, Merega E, Milanese M, Summa M, Casazza S, Raffaghello L, Pistoia V, Uccelli A, Pittaluga A (2013) CCL5-glutamate interaction in central nervous system: Early and acute presynaptic defects in EAE mice. Neuropharmacology 75:337–346
34. Subramanian J, Morozov A (2013) Erk1/2 inhibit synaptic vesicle exocytosis through L-type calcium channels. J Neurosci 31(12): 4755–4764
35. Vara H, Onofri F, Benfenati F, Sassoe-Pognetto M, Giustetto M (2009) ERK activation in axonal varicosities modulates presynaptic plasticity in the CA3 region of the hippocampus through synapsin I. Proc Natl Acad Sci U S A 106(24):9872–9877
36. Giachello CN, Fiumara F, Giacomini C, Corradi A, Milanese C, Ghirardi M, Benfenati F, Montarolo PG (2010) MAPK/Erk-dependent phosphorylation of synapsin mediates formation of functional synapses and short-term homosynaptic plasticity. J Cell Sci 123(Pt 6):881–893
37. Chi P, Greengard P, Ryan TA (2001) Synapsin dispersion and reclustering during synaptic activity. Nat Neurosci 4(12):1187–1193. doi:10.1038/nn756
38. Marra V, Burden JJ, Thorpe JR, Smith IT, Smith SL, Hausser M, Branco T, Staras K (2012) A preferentially segregated recycling vesicle pool of limited size supports neurotransmission in native central synapses. Neuron 76(3):579–589
39. Cousin MA, Robinson PJ (2001) The dephosphins: dephosphorylation by calcineurin triggers synaptic vesicle endocytosis. Trends Neurosci 24(11):659–665
40. Shin T, Ahn M, Jung K, Heo S, Kim D, Jee Y, Lim YK, Yeo EJ (2003) Activation of mitogen-activated protein kinases in experimental autoimmune encephalomyelitis. J Neuroimmunol 140(1–2):118–125
41. Zhu D, Wu X, Strauss KI, Lipsky RH, Qureshi Z, Terhakopian A, Novelli A, Banaudha K, Marini AM (2005) *N*-methyl-D-aspartate and TrkB receptors protect neurons against glutamate excitotoxicity through an extracellular signal-regulated kinase pathway. J Neurosci Res 80(1):104–113. doi:10.1002/jnr.20422
42. Fang XX, Jiang XL, Han XH, Peng YP, Qiu YH (2013) Neuroprotection of interleukin-6 against NMDA-induced neurotoxicity is mediated by JAK/STAT3, MAPK/ERK, and PI3K/AKT signaling pathways. Cell Mol Neurobiol 33(2):241–251. doi:10.1007/s10571-012-9891-6
43. Almeida RD, Manadas BJ, Melo CV, Gomes JR, Mendes CS, Grãos MM, Carvalho RF, Carvalho AP, Duarte CB (2005) Neuroprotection by BDNF against glutamate-induced apoptotic cell death is mediated by ERK and PI3-kinase pathways. Cell Death Differ 12(10):1329–1343. doi:10.1038/sj.cdd.4401662
44. Sama DM, Norris CM (2013) Calcium dysregulation and neuroinflammation: discrete and integrated mechanisms for age-related synaptic dysfunction. Ageing Res Rev 12(4):982–995. doi:10.1016/j.arr.2013.05.008
45. Alvarez S, Blanco A, Fresno M, Muñoz-Fernández M (2011) TNF-α contributes to caspase-3 independent apoptosis in neuroblastoma cells: role of NFAT. PLoS One 6(1):e16100. doi:10.1371/journal.pone.0016100
46. Potluri K, Holt D, Hou S (2014) Neurologic complications in renal transplantation. Handb Clin Neurol 121:1245–1255. doi:10.1016/B978-0-7020-4088-7.00084-5
47. Wallis JD (2012) Cross-species studies of orbitofrontal cortex and value-based decision-making. Nat Neurosci 15(1):13–19. doi:10.1038/nn.2956
48. Seamans JK, Lapish CC, Durstewitz D (2008) Comparing the prefrontal cortex of rats and primates: insights from electrophysiology. Neurotox Res 14(2–3):249–262. doi:10.1007/BF03033814
49. Rudebeck PH, Walton ME, Millette BH, Shirley E, Rushworth MF, Bannerman DM (2007) Distinct contributions of frontal areas to emotion and social behaviour in the rat. Eur J Neurosci 26(8): 2315–2326. doi:10.1111/j.1460-9568.2007.05844.x
50. Chudasama Y, Robbins TW (2006) Functions of frontostriatal systems in cognition: comparative neuropsychopharmacological studies in rats, monkeys and humans. Biol Psychol 73(1):19–38. doi:10.1016/j.biopsycho.2006.01.005
51. Chaudhuri A, Behan PO (2000) Fatigue and basal ganglia. J Neurol Sci 179(S 1-2):34–42
52. Bakshi R (2003) Fatigue associated with multiple sclerosis: diagnosis, impact and management. Mult Scler 9(3):219–227
53. Pardini M, Bonzano L, Roccatagliata L, Mancardi GL, Bove M (2013) The fatigue-motor performance paradox in multiple sclerosis. Sci Rep 3:2001. doi:10.1038/srep02001
54. Pardini M, Bonzano L, Mancardi GL, Roccatagliata L (2010) Frontal networks play a role in fatigue perception in multiple sclerosis. Behav Neurosci 124(3):329–336. doi:10.1037/a0019585
55. Tecchio F, Zito G, Zappasodi F, Dell' Acqua ML, Landi D, Nardo D, Lupoi D, Rossini PM, Filippi MM (2008) Intra-cortical connectivity in multiple sclerosis: a neurophysiological approach. Brain 131(Pt 7): 1783–1792. doi:10.1093/brain/awn087
56. Maarouf A, Audoin B, Konstandin S, Rico A, Soulier E, Reuter F, Le Troter A, Confort-Gouny S, Cozzone PJ, Guye M, Schad LR, Pelletier J, Ranjeva JP, Zaaraoui W (2014) Topography of brain sodium accumulation in progressive multiple sclerosis. MAGMA 27(1):53–62. doi:10.1007/s10334-013-0396-1
57. Roelcke U, Kappos L, Lechner-Scott J, Brunnschweiler H, Huber S, Ammann W, Plohmann A, Dellas S, Maguire RP, Missimer J, Radü EW, Steck A, Leenders KL (1997) Reduced glucose metabolism in the frontal cortex and basal ganglia of multiple sclerosis patients with fatigue: a 18F-fluorodeoxyglucose positron emission tomography study. Neurology 48(6):1566–1571
58. Mandolesi G, Grasselli G, Musumeci G, Centonze D (2010) Cognitive deficits in experimental autoimmune encephalomyelitis: neuroinflammation and synaptic degeneration. Neurol Sci 31(Suppl 2):S255–S259. doi:10.1007/s10072-010-0369-3